Supplementary Online Material for
"The Rhone Glacier was smaller than today for most of the Holocene"

Geological Setting

During the Last Glacial Maximum (LGM), the Swiss Alps were covered, with the exception of the highest peaks, by a large ice cap consisting of a few main domes and outlet glaciers (Kelly et al., 2004). These LGM glaciers and previous glaciations contributed to the classic alpine topography seen today. The Rhone Glacier, forming the headwaters of the Rhone River, was one of the largest outlet glaciers. Since the Egesen Stade, the Rhone Glacier has retreated into its modern valley and has since re-expanded into the Rhone Valley during the Little Ice Age (Fig. DR1). Since the termination of the Little Ice Age in the mid 19th century, the Rhone Glacier has retreated above a large riegel (Fig. DR1).

Figure DR1. Images showing the extent of the Rhone Glacier in 1900 CE, approximately 50 years after the Little Ice Age maximum, and CE2008. The terminus has retreated up the large riegel and now sits within a small over-deepening. During the LIA the sample surfaces were buried by the Rhone Glacier with a thickness of ≥ 60 m, ceasing cosmogenic nuclide production. Images courtesy of Glaciers Online (http://www.swisseduc.ch/glaciers/alps/rhonegletscher/index-en.html, access date January 25, 2011).

The Rhone Glacier is a natural test-bed for the $^{14}C/^{10}Be$ method presented here as it is one of the largest remaining glaciers in the Swiss Alps and is known to respond sensitively to climate changes (Stroeven et al., 1989; Wallinga and van de Wal, 1998). Its history is also well documented. In front of the Rhone Glacier terminus, clean, washed bedrock is extensively exposed. Samples were taken from bedrock surfaces, typically from the tops of roche moutonnée type features. Most of the bedrock samples were exposed by the retreating Rhone Glacier in 2005-2006 CE and are currently approximately 30 m from the ice front (Table DR1; Fig. DR2).

Figure DR2. Photograph of typical sampled surface (Rho-2). All samples are from striated and polished bedrock. Samples are from no more than 30 m in front of modern glacier terminus and were buried by the glacier as late as 2006 CE. Many of the sampled surfaces are from the tops of roche moutonnée type features. We sampled abraded surfaces only, avoiding surfaces showing evidence for former quarrying processes.

Materials and Methods

$^{14}C/^{10}Be$ Burial Dating

In situ ^{14}C is a new isotopic tool (Lifton et al., 2001) that can be used to understand the exposure history of a geomorphic surface. The systematics of *in situ* ^{14}C production is similar to ^{10}Be and can be used for simple exposure dating (see below). Because of its short (5730 year) half-life, *in situ* ^{14}C is arguably most useful when combined with other long-lived or stable cosmogenic nuclides, such as ^{10}Be (1.387±0.012 Myr; Anderson et al., 2008; Chmeleff et al., 2010; Korschinek et al., 2010; Miller et al., 2006). During periods of exposure to cosmic rays, ^{14}C and ^{10}Be are produced in the quartz phase of the granitic bedrock underlying the Rhone Glacier at an initial ratio of about 3.2 for production by fast neutron spallation (Dugan et al., 2008; Lifton et al., 2001). Inclusion of production by muons increases the initial $^{14}C/^{10}Be$ ratio because the fraction of ^{14}C produced by muons is greater than the comparable fraction for ^{10}Be (Heisinger et al., 2002a; Heisinger et al., 2002b). The evolution of the $^{14}C/^{10}Be$ ratio decreases with exposure time, even for continuous exposure (Fig. DR3). During ice extents greater than today, sampled bedrock surfaces were buried by many meters of ice >100 m during LIA (Fig. DR1). During these periods of burial, the $^{14}C/^{10}Be$ ratio decays as a function of the burial time with essentially the half-life of ^{14}C. Therefore if the measured $^{14}C/^{10}Be$ ratio is below the production ratio, we can estimate the duration of burial by ice, in addition to exposure.

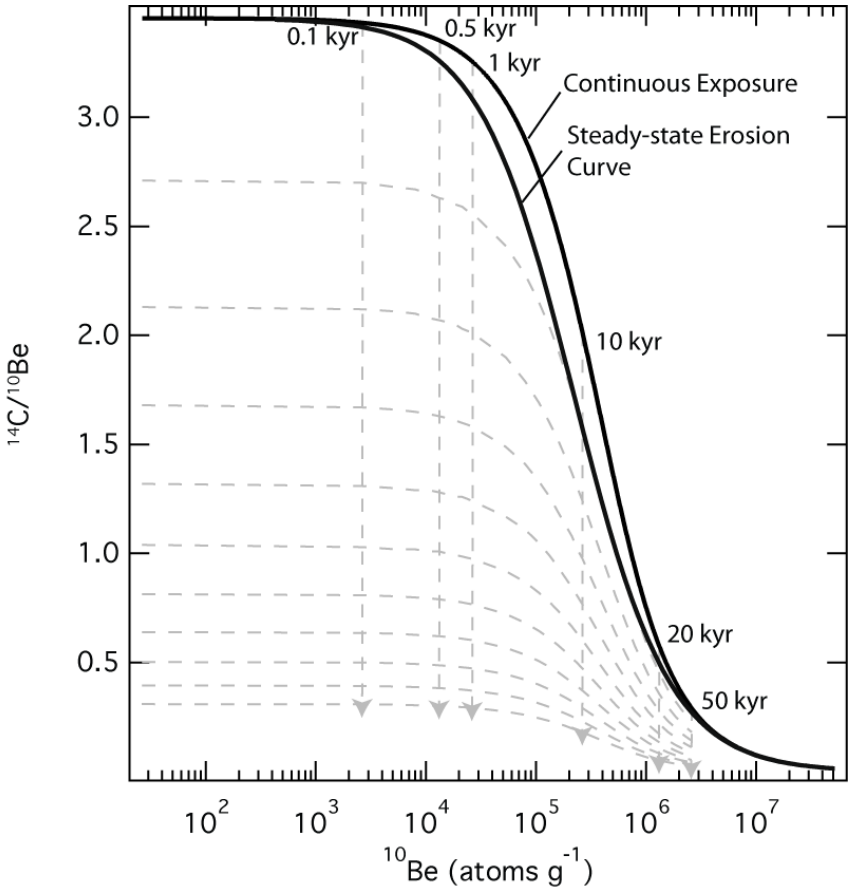

Figure DR3. ^{14}C-^{10}Be paired-isotope plot showing the evolution of the $^{14}C/^{10}Be$ ratio versus ^{10}Be concentration. Upper heavy black curve represents evolution under continuous exposure and zero erosion. Lower heavy black curve defines field of continuous exposure with steady-state erosion. Exposure time increases to the right along the curves, example exposure durations indicated by labeled vertical dashed lines; burial duration increases vertically downwards along vertical dashed lines.

The $^{14}C/^{10}Be$ ratio is primarily controlled by the exposure and burial history. The absolute concentration of ^{10}Be is a function of exposure time and amount of glacial erosion during burial, decay of ^{10}Be is negligible during the relatively short time-scales (~10 ka) discussed here. The concentration of ^{14}C is a function of exposure, burial, and erosion. Note, that decay of the $^{14}C/^{10}Be$ ratio during burial is not simply a function of burial duration in this case because of the assumption of erosion during burial and the non-constant nature of $^{14}C/^{10}Be$ ratio with depth when muogenic production is included (Fig. DR4).

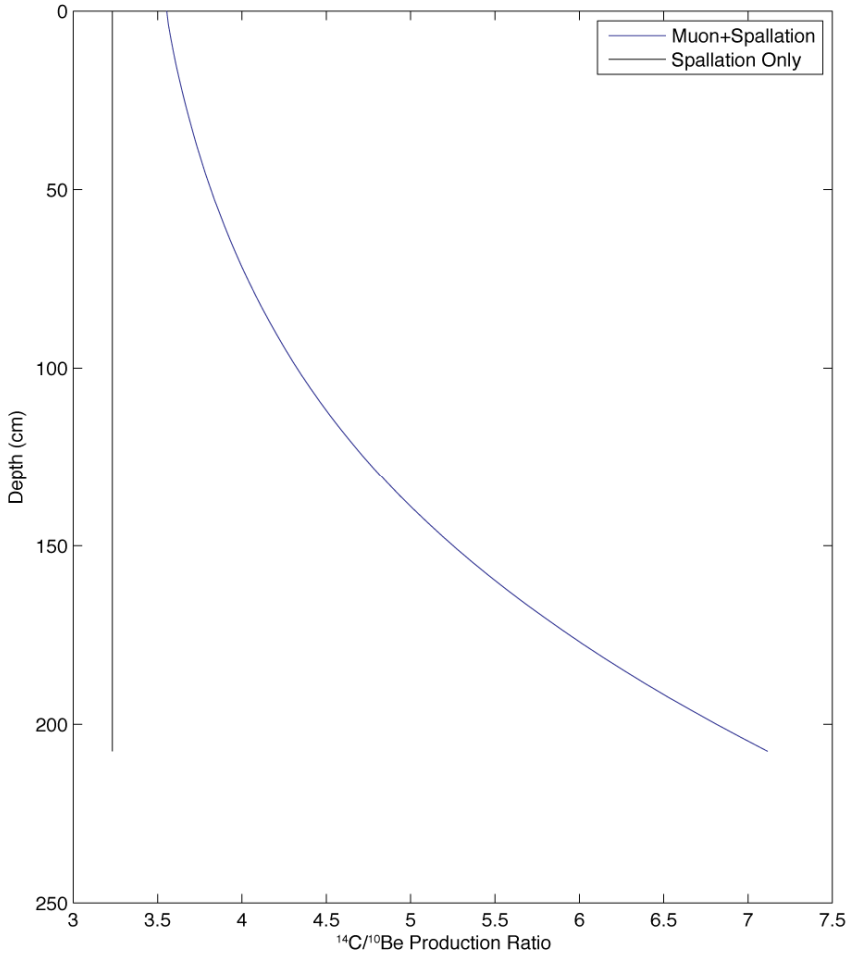

Figure DR4. $^{14}C/^{10}Be$ depth profile at ~46°N, 8.5°E, and 2250 m elevation, typical of our samples, for spallation only (black line) and spallation+muogenic production (blue line).

^{10}Be and ^{14}C Production Rates

We have adopted the ^{10}Be production rates presented in Balco et al. (2009) from Late Glacial moraines in northeastern North America. ^{14}C rates are based on data presented in Lifton et al. (2001) and Dugan et al. (2008). The production rate measurements in these studies are derived from pluvial Lake Bonneville shorelines in Utah and supra-glacial landslide deposits in northwest Scotland. We also adopt the scaling model presented in Lifton et al. (2005) and average the production rates over the last 10 kyr. The sea level high latitude ^{10}Be and ^{14}C spallation production rates used in this study are therefore 4.5±0.2 ^{10}Be at g^{-1} yr^{-1} (relative to 07KNSTD3110 with a $^{10}Be/^{9}Be$ ratio of 2.85 x 10^{-12}) and 14.4±0.5 ^{14}C at g^{-1} yr^{-1}, respectively, yielding a $^{14}C/^{10}Be$ production ratio for spallation of 3.2±0.2). Production by muons is independently calculated based on the cross-sections presented in Heisinger et al. (2002a; 2002b). The choice of ^{14}C and ^{10}Be production rates, as well as the scaling model employed, has

little impact (<10%) on the results or conclusions drawn from the ^{14}C and ^{10}Be measurements.

Analytical Methods

***In situ* ^{14}C:** Extraction of ^{14}C was carried out at the Lamont-Doherty Earth Observatory *in situ* ^{14}C Laboratory, following the methods of Lifton et al. (2001) and Pigati (2004). ^{14}C activities were measured at the University of Arizona Accelerator Mass Spectrometry Facility. Measured ^{14}C activities are corrected for $\delta^{13}C$ differences from the Oxalic Acid ^{14}C Standard used for measurement. A five-gram split of the quartz used for ^{10}Be analysis was fused in a 50 torr research grade O_2 atmosphere (Table DR2). Procedural blank measurements were made before and after a series of samples and the long-term average of the number of ^{14}C atoms (3.36±0.83 and 1.57±0.28 x 10^5 ^{14}C at) in the procedural blanks was subtracted from each sample (Tables DR3-DR5). The samples measured in 2010 show a lower and better-constrained blank, while the samples measured during 2009 have a higher blank with more analytical uncertainty (Table DR3). Because the blank correction is considerable (15-65%), we have placed more emphasis on the more robust ^{14}C measurements performed in 2010.

^{10}Be: Chemical processing for ^{10}Be was carried out in the Lamont-Doherty Earth Observatory Cosmogenic Nuclide Laboratory following routine beryllium isolation methods (http://www.ldeo.columbia.edu/tcn/), which is based on the procedures used at the University of Washington (http://depts.washington.edu/cosmolab/chem.html). We used a low-level Be-carrier ($^{10}Be/^{9}Be \sim 10^{-16}$). All $^{10}Be/^{9}Be$ ratios (Table DR2) were measured at the Lawrence-Livermore National Laboratory Center for Accelerator Mass Spectrometry relative to the 07KNSTD3110 standard with a ratio of 2.85 x 10^{-12} (Nishiizumi et al., 2007) and corrected for background $^{10}Be/^{9}Be$ given by the procedural blanks, residual boron contamination, and machine background (all background $^{10}Be/^{9}Be$ ratios were less than $2x10^{-15}$).

Method Assumptions

Last Ice Age glaciation reset alpine bedrock: We base our calculations on the assumption that the large glaciations of the last ice-age, lasting for many tens of thousands of years, 'reset' the cosmogenic clock in the sampled bedrock surfaces (i.e. that the cosmogenic inventory of subglacial bedrock was zero at the end of the late glacial period about 12 kyr ago). We conservatively assume the total erosion of the Rhone Glacier, including abrasion and quarrying processes, integrated over the entire last glacial cycle at the sampling sites to be on the order of meters. We quantitatively verified this assumption by measuring the cosmogenic nuclide ^{26}Al in some of our samples. The half-life of ^{26}Al is approximately 717 kyr (http://www.nndc.bnl.gov/chart/, access date January 25, 2011). If ^{26}Al and ^{10}Be were produced in the sampled bedrock prior to the last glacial cycle, the ^{26}Al ages would show discordance from the ^{10}Be ages due to more rapid decay of ^{26}Al than ^{10}Be during the extended periods of burial during the last glacial cycle. On the other hand, if all cosmogenic nuclides produced prior to the last glacial cycle were removed from the bedrock via erosion, and all the measured cosmogenic nuclides were produced during the Holocene, ^{26}Al and ^{10}Be ages would agree. Results for samples Rho-1, -2, -3, and -4 show general concordance between the ^{10}Be and ^{26}Al age (Fig. DR5; Tables DR1 and DR5), which suggests that any previous exposure was removed by glacial erosion and that the measured ^{10}Be was produced during the Holocene period.

All samples experienced same ex posure/burial history: Based on geomorpho-stratigraphic arguments that are independently confirmed by the multi-isotope data, we assume that all samples experienced the same exposure and burial history. This assumption is generally confirmed by consistent $^{14}C/^{10}Be$ ratios of samples Rho-6 through Rho-11 (Table DR1). The greater scatter in the $^{14}C/^{10}Be$ ratios of samples Rho-1 through Rho-5 is most likely due to the higher ^{14}C blank correction (see above).

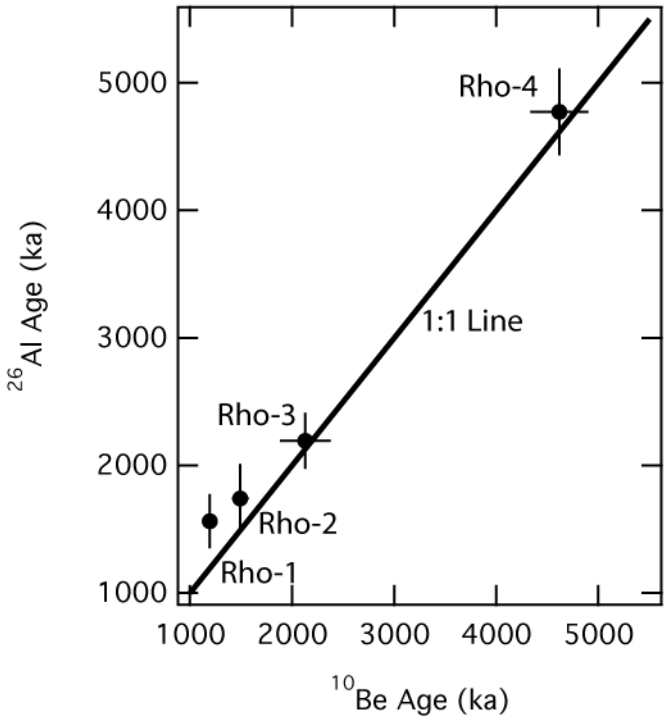

Figure DR5. Plot of ^{26}Al versus ^{10}Be age showing general concordance between the two nuclides, supporting the scenario that the bedrock surfaces were reset with respect to their cosmogenic nuclide inventory during the last glacial cycle (see Tables DR1 and DR5 and main text). Uncertainties are shown at 1σ level. All samples overlap with 1:1 line at 2σ.

^{14}C and ^{10}Be production by muons during periods of burial is negligible: Production of ^{10}Be and ^{14}C by fast-neutron spallation is rapidly attenuated with depth in earth surface materials; however, production by muons is much less strongly attenuated at depth. Therefore, during typical periods of burial (~60 m of ice) production of both ^{10}Be and ^{14}C is effectively zero. As a test of the sensitivity of our results to production by muons during burial, we adopt an unlikely scenario of burial by only 10 m of ice for 1000 years. Results are a ^{10}Be production rate (includes spallation and muons) of 0.05 at g^{-1} yr^{-1} and 0.8 at g^{-1} yr^{-1} for ^{14}C. The integrated production of both these nuclides for 1000 years, even disregarding decay of ^{14}C, is ≤ 1 % of the measured ^{14}C concentration and ≤ 2 % for ^{10}Be, both of which are within the 1σ uncertainties of the measurements. We conclude that production by muons has negligible effects for this study.

Exposure, Burial and Erosion Rate Calculations

The burial durations (t_b) and erosion depths (E) for each sample can be determined by:

$$N_{10}(t_b,E)=\left[P_{10_{sp}}e^{-E/\Lambda_{sp}}+P_{10_{\mu^-}}e^{-E/\Lambda_{\mu^-}}+P_{10_{\mu_{fast}}}e^{-E/\Lambda_{\mu fast}}\right]\frac{1}{\lambda_{10}}\left(1-e^{-(t_i-t_b)\lambda_{10}}\right)e^{-\lambda_{10}t_b} \quad \text{(S1)},$$

and:

$$R_{\frac{14}{10}}(t_b,E)=\frac{\left[P_{14_{sp}}e^{-E/\Lambda_{sp}}+P_{14_{\mu^-}}e^{-E/\Lambda_{\mu^-}}+P_{14_{\mu_{fast}}}e^{-E/\Lambda_{\mu fast}}\right]\frac{1}{\lambda_{14}}\left(1-e^{-(t_i-t_b)\lambda_{14}}\right)e^{-t_b\lambda_{14}}}{\left[P_{10_{sp}}e^{-E/\Lambda_{sp}}+P_{10_{\mu^-}}e^{-E/\Lambda_{\mu^-}}+P_{10_{\mu_{fast}}}e^{-E/\Lambda_{\mu fast}}\right]\frac{1}{\lambda_{10}}\left(1-e^{-(t_i-t_b)\lambda_{10}}\right)e^{-t_b\lambda_{10}}} \quad \text{(S2)}.$$

N_{10} is the measured ^{10}Be concentration, $R_{14/10}$ is the measured ^{14}C/^{10}Be ratio, P_{10sp}, $P_{10\mu^-}$, and $P_{10\mu fast}$ are the ^{10}Be production rates for spallation, negative muons, and fast muons, respectively, with similar terms for ^{14}C. Λ_{sp}, Λ_{μ^-}, and $\Lambda_{\mu fast}$ are the attenuation lengths of the three production pathways. λ_{10} and λ_{14} are the ^{10}Be and ^{14}C decay constants. However, the long half life of ^{10}Be (1.387 Myr; Chmeleff et al., 2010; Korschinek et al., 2010) relative to the length of Holocene (11,500 yr) means that <<1% of the ^{10}Be decays during any burial period and therefore can be ignored. Equation S1 therefore simplifies to:

$$N_{10}(t_b,E)=\left[P_{10_{sp}}e^{-E/\Lambda_{sp}}+P_{10_{\mu^-}}e^{-E/\Lambda_{\mu^-}}+P_{10_{\mu_{fast}}}e^{-E/\Lambda_{\mu fast}}\right](t_i-t_b) \quad \text{(S3)},$$

and similarly Equation S2 simplifies to:

$$R_{\frac{14}{10}}(t_b,E)=\frac{\left[P_{14_{sp}}e^{-E/\Lambda_{sp}}+P_{14_{\mu^-}}e^{-E/\Lambda_{\mu^-}}+P_{14_{\mu_{fast}}}e^{-E/\Lambda_{\mu fast}}\right]\frac{1}{\lambda_{14}}\left(1-e^{-(t_i-t_b)\lambda_{14}}\right)e^{-t_b\lambda_{14}}}{\left[P_{10_{sp}}e^{-E/\Lambda_{sp}}+P_{10_{\mu^-}}e^{-E/\Lambda_{\mu^-}}+P_{10_{\mu_{fast}}}e^{-E/\Lambda_{\mu fast}}\right](t_i-t_b)} \quad \text{(S4)}.$$

The erosion depths (E) for each sample can then be determined by substitution of S3 into S4. Burial durations are then determined from S3. The exposure duration (t_e) is determined based on the assumed initial exposure age (t_i; see main text) and is the difference between the initial exposure age and burial duration.

Supporting Data Tables

Table DR1. ^{10}Be and ^{14}C sample data. Columns are sample latitude, longitude, and elevation. Concentration of ^{10}Be and ^{14}C, corrected for background, equivalent apparent ^{10}Be and ^{14}C exposure ages, and ^{14}C/^{10}Be ratio. All uncertainties reported at 1σ.

Sample	Latitude (N)	Longitude (E)	Elevation (m a.s.l.)	Thickness (cm)	Topographic Shielding	^{10}Be[1] (10^4 at g^{-1})	^{14}C[1] (10^4 at g^{-1})	^{10}Be Age[2] (ka)	^{14}C Age[2] (ka)	^{14}C/^{10}Be
Rho-1	46.5787	8.3843	2220	2.24	0.983	2.81±0.06	6.98±2.01	1.19±0.07	0.89±0.16	2.51±0.43
Rho-2	46.5788	8.3845	2227	2.17	0.984	3.55±0.08	6.69±2.42	1.49±0.08	0.85±0.23	1.91±0.48
Rho-3	46.5787	8.3847	2230	1.84	0.965	5.10±0.53	10.62±2.17	2.13±0.25	1.37±0.20	2.1±0.35
Rho-4	46.5785	8.3852	2244	3.04	0.970	11.21±0.40	20.36±2.25	4.62±0.29	2.83±0.27	1.82±0.15
Rho-5	46.57887	8.38375	2211	1.05	0.982	0.25±0.02	1.68±1.30	0.11±0.01	0.21±0.16	6.63±4.97
Rho-6	46.57887	8.38375	2211	1.97	0.982	5.99±0.11	7.49±1.24	2.59±0.14	0.97±0.18	1.25±0.22
Rho-7	46.57897	8.38447	2224	2.40	0.985	5.48±0.11	7.69±1.24	2.35±0.13	0.99±0.17	1.4±0.23
Rho-8	46.5789	8.38529	2241	2.64	0.985	9.36±0.18	12.06±1.24	3.92±0.21	1.58±0.19	1.29±0.13
Rho-9	46.57861	8.38564	2259	1.86	0.993	9.83±0.19	13.18±1.28	4.01±0.21	1.69±0.19	1.34±0.13
Rho-10	46.57871	8.38746	2308	1.77	0.960	11.00±0.21	15.12±1.24	4.46±0.24	1.96±0.20	1.37±0.12
Rho-11	46.57854	8.38690	2294	2.30	0.960	13.00±0.29	18.43±1.66	5.33±0.29	2.50±0.22	1.42±0.1

[1] Corrected for background ^{10}Be and ^{14}C. See Table DR3 for background measurements.

[2] Calculated using variable production rate due to variable geomagnetic field in the CRONUS-Earth calculator, but modified for ^{14}C age calculation (Balco et al., 2008). Ages assume continuous exposure with no erosion. Uncertainties include analytical uncertainties only.

Table DR2. ^{10}Be and ^{14}C sample data details. Columns are mass of Be carrier, measured ^{10}Be/^{9}Be ratio, mass of quartz digested for ^{10}Be measurement, mass of quartz fused for ^{14}C measurement, volume of CO_2 extracted from^{14}C quartz aliquot, equivalent mass of carbon, volume of diluted CO_2 after sample extraction, the fraction modern ^{14}C measured in the diluted CO_2, number of ^{14}C atoms measured prior to correction for ^{14}C background, and associated ^{10}Be and ^{14}C blanks used to asses background. All uncertainties reported at 1σ.

Sample	Be Carrier (g)	^{10}Be/^{9}Be (10^{-14})	^{10}Be Sample Mass (g)	^{14}C Sample Mass (g)	V_{CO2} (10^{-2} cc STP)	Mass C (μg)	$V_{Diluted}$ (cc STP)	F_m Measured	^{14}C Sample[1] (10^{5} at)	% ^{14}C Blank Correction	^{10}Be Blank	^{14}C Blank
Rho-1	0.2531	8.56±0.19	50.7141	5.0004	5.18±0.06	27.74	1.69±0.02	0.0128±0.0016	6.87±0.86	48.9	B2-5-07	2009 Blanks
Rho-2	0.2527	10.79±0.22	50.7466	5.0081	4.39±0.05	23.50	1.67±0.02	0.0127±0.0020	6.71±1.04	50.1	B2-5-07	2009 Blanks
Rho-3	0.2534	15.44±1.60	50.8163	5.0606	4.74±0.05	25.36	1.66±0.02	0.0167±0.0017	8.74±0.92	38.4	B2-5-07	2009 Blanks
Rho-4	0.2534	34.53±1.23	51.8476	5.0226	3.77±0.04	20.17	1.63±0.02	0.0263±0.0018	13.56±0.95	24.8	B2-5-07	2009 Blanks
Rho-5	0.1984	0.69±0.05	31.1979	5.20460	3.47±0.04	18.56	1.52±0.02	0.0050±0.0012	2.43±0.58	64.6	Blank09Dec11	2010 Blanks
Rho-6	0.2009	23.96±0.39	53.2692	5.08510	3.88±0.04	20.76	1.51±0.02	0.0112±0.0012	5.35±0.59	29.4	Blank09Dec11	2010 Blanks
Rho-7	0.1992	20.69±0.37	49.8733	5.13470	6.08±0.07	32.58	1.49±0.02	0.0117±0.0012	5.49±0.57	28.6	Blank09Dec11	2010 Blanks
Rho-8	0.2004	34.64±0.56	49.2522	5.01770	2.14±0.02	11.48	1.43±0.02	0.0168±0.0012	7.61±0.55	20.6	Blank09Dec11	2010 Blanks
Rho-9	0.2002	30.98±0.50	41.8802	5.07370	2.55±0.03	13.66	1.42±0.02	0.0183±0.0012	8.23±0.56	19.1	Blank09Dec11	2010 Blanks
Rho-10	0.1999	42.62±0.69	51.2652	5.03760	2.99±0.03	16.01	1.42±0.02	0.0205±0.0013	9.16±0.58	17.1	Blank09Dec11	2010 Blanks
Rho-11	0.2004	49.50±0.99	50.5339	5.07370	3.40±0.04	18.22	1.40±0.02	0.0246±0.0012	10.88±0.56	14.4	Blank09Dec11	2010 Blanks

[1] Not corrected for background.

Table DR3. ^{14}C blank data. V_{CO2} is the volume of CO_2 collected during blank extraction, Mass C is the mass of carbon extracted, $V_{Diluted}$ is the volume of the diluted gas prior to AMS and $\delta^{13}C$ splitting, and F_m is the fraction modern ^{14}C value of the diluted gas. All uncertainties reported at 1σ.

Blank ID	V_{CO2} (10^{-2} cc STP)	Mass C (μg)	$V_{Diluted}$ (cc STP)	F_m Measured	^{14}C Blank (10^5 at)
Blank1-26-09	1.50±0.02	8.01±0.09	1.28±0.01	0.0075±0.0012	2.13±0.68
Blank2-16-09	1.91±0.02	10.21±0.12	1.59±0.02	0.0097±0.0012	3.91±0.84
				Average	3.36±0.83
Blank1-18-10	1.73±0.01	9.24±0.08	2.52±0.02	0.0035±0.0002	1.7±0.93
Blank2-8-10	1.52±0.02	8.16±0.09	1.47±0.02	0.0051±0.0003	1.44±0.56
Blank 3-5-10	1.24±0.01	6.63±0.08	1.14±0.01	0.0057±0.0002	1.33±0.43
Blank 3-29-10	1.78±0.02	9.54±0.11	1.37±0.02	0.0059±0.0002	1.79±0.51
				Average	1.57±0.28

Table DR4. ^{10}Be blank data. Mass of Be carrier, measured $^{10}Be/^{9}Be$ ratio, and resulting number of ^{10}Be atoms in blank. All uncertainties reported at 1σ.

Blank ID	Be Carrier (g)	$^{10}Be/^{9}Be$ (10^{-15})	^{10}Be (10^4 at)
B2-5-07	0.2524	1.06±1.06	1.77±1.79
Blank09Dec11	0.2012	0.87±0.14	1.17±0.19

Table DR5. ^{26}Al data. Mass of quartz digested for ^{26}Al measurement, total Al in digested quartz (note no carrier Al added to samples), measured $^{26}Al/^{27}Al$ ratio, ^{26}Al concentration, and resulting apparent ^{26}Al exposure age. All uncertainties reported at 1σ.

Sample	Sample Mass (g)	Total Al (mg)	$^{26}Al/^{27}Al$ (10^{-13})	^{26}Al (10^5 at g^{-1})	^{26}Al Age (ka)
Rho-1	50.7141	2.73±0.02	2.12±0.29	**2.55±0.34**	1.56±0.21
Rho-2	50.7466	3.09±0.02	2.10±0.33	**2.85±0.45**	1.74±0.27
Rho-3	50.8163	3.05±0.04	2.70±0.27	**3.62±0.36**	2.19±0.22
Rho-4	51.8476	2.89±0.03	6.40±0.45	**7.97±0.57**	4.77±0.34

Table DR6. Calculated exposure durations, burial durations, and erosion rates.

Sample	Exposure Duration (kyr)	Burial Duration (kyr)	Erosion Depth (cm)	Equivalent Erosion Rate (mm yr^{-1})[1]
Rho-1	9.12±1.62	1.88±0.33	145±26	0.33±0.151
Rho-2	7.19±1.85	3.81±0.98	112±29	0.25±0.125
Rho-3	9.00±1.54	2.00±0.34	102±18	0.23±0.106
Rho-4	9.02±0.84	1.98±0.18	47±4	0.11±0.046
Rho-5	--	--	291±30 [3]	0.66±0.29 [3]
Rho-6	3.87±0.70	7.13±1.28	31±6	0.07±0.032
Rho-7	4.97±0.84	6.03±1.02	54±9	0.12±0.056
Rho-8	4.73±0.54	6.27±0.71	14±2	0.03±0.014
Rho-9	5.24±0.56	5.76±0.61	19±2	0.04±0.019
Rho-10	5.66±0.55	5.34±0.52	14±1	0.03±0.014
Rho-11	6.21±0.52	4.79±0.40	9±1	0.02±0.009
Average[2]	**6.49±1.96**	**4.50±1.96**	--	--

[1] Erosion rates calculated using the average burial duration based on all samples.
[2] Average is arithmetic mean and standard deviation of all samples, except for Rho-5.
[3] Calculated using ^{10}Be concentration and mean exposure and burial duration.

References

Anderson, R. K., Miller, G. H., Briner, J. P., Lifton, N. A., and DeVogel, S. B., 2008, A millennial perspective of Arctic warming from ^{14}C in quartz and plants emerging from beneath ice caps: Geophys. Res. Lett., v. 35, no. L01502, p. doi: 10.1029/2007GL03057.

Balco, G., Briner, J., Finkel, R. C., Rayburn, J. A., Ridge, J. C., and Schaefer, J. M., 2009, Regional beryllium-10 production rate calibration for late-glacial northeastern North America: Quaternary Geochronology, v. 4, no. 2, p. 93-107.

Balco, G., Stone, J., Lifton, N. A., and Dunai, T. J., 2008, A complete and easily accessible means of calculating surface exposure ages or erosion rates from ^{10}Be and ^{26}Al measurements: Quaternary Geochronology, v. 3, no. 3, p. 174-195.

Chmeleff, J., Blanckenburg, F. v., Kossert, K., and Jakob, D., 2010, Determination of the 10Be half-life by multicollector ICP-MS and liquid scintillation counting: Nuclear Inst. and Methods in Physics Research, B, v. 268, no. 2, p. 192-199.

Dugan, B., Lifton, N., and Jull, A. J. T., 2008, New production rate estimates for in situ cosmogenic C-14: Geochim. Cosmochim. Acta, v. 72, no. 12, p. A231-A231.

Heisinger, B., Lal, D., Jull, A. J. T., Kubik, P., Ivy-Ochs, S., Knie, K., and Nolte, E., 2002a, Production of selected cosmogenic radionuclides by muons: 2. Capture of negative muons: Earth and Planetary Science Letters, v. 200, p. 357-369.

Heisinger, B., Lal, D., Jull, A. J. T., Kubik, P., Ivy-Ochs, S., Neumaier, S., Knie, K., Lazarev, V., and Nolte, E., 2002b, Production of selected cosmogenic radionuclides by muons: 1. Fast muons: Earth and Planetary Science Letters, v. 200, p. 345-355.

Kelly, M. A., Buoncristiani, J.-F., and Schlüchter, C., 2004, A reconstruction of the last glacial maximum (LGM) ice-surface geometry in the western Swiss Alps and

contiguous Alpine regins in Italy and France: Eclogae geologicae Helvtiae, v. 97, p. 57-75.

Korschinek, G., Bergmaier, A., Faestermann, T., Gerstmann, U. C., Knie, K., Rugel, G., Wallner, A., Dillmann, I., Dollinger, G., Gostomski, C. L. v., Kossert, K., Maiti, M., Poutivtsev, M., and Remmert, A., 2010, A new value for the half-life of 10Be by Heavy-Ion Elastic Recoil Detection and liquid scintillation counting: Nuclear Inst. and Methods in Physics Research, B, v. 268, no. 2, p. 187-191.

Lifton, N. A., Bieber, J. W., Clem, J. M., Duldig, M. L., Evenson, P., Humble, J. E., and Pyle, R., 2005, Addressing solar modulation and long-term uncertainties in scaling secondary cosmic rays for in situ cosmogenic nuclide applications: Earth and Planetary Science Letters, v. 239, p. 140-161.

Lifton, N. A., Jull, A. J. T., and Quade, J., 2001, A new extraction technique and production rate estimate for in situ cosmogenic ^{14}C in quartz: Geochimica et Cosmochimica Acta, v. 65, no. 12, p. 1953-1969.

Miller, G. H., Briner, J. P., Lifton, N. A., and Finkel, R. C., 2006, Limited ice-sheet erosion and complex exposure histories derived from in situ cosmogenic ^{10}Be, ^{26}Al, and ^{14}C on Baffin Island, Arctic Canada: Quaternary Geochronology, v. 1, no. 1, p. 74-85.

Nishiizumi, K., Imamura, M., Caffee, M. W., Southon, J. R., Finkel, R. C., and McAninch, J., 2007, Absolute calibration of ^{10}Be AMS standards: Nuclear Instruments and Methods in Physics Research B, v. 258, p. 403-413.

Pigati, J. S., 2004, Experimental Developments and Application of Carbon-14 and in situ Cosmogenic Nuclide Dating Techniques [PhD thesis]: University of Arizona, 188 p.

Stroeven, A., van de Wal, R., and Oerlemans, J., 1989, Historic Front Variations of the Rhone Glacier: Simulation with an Ice Flow Model, *in* Oerlemans, J., ed., Glacier Fluctuations and Climatic Change: Dordrecht, Kluwer Academic Publishers.

Wallinga, J., and van de Wal, R. S. W., 1998, Sensetivity of Rhonegletscher, Switzerland, to climate change: experiments with a one-dimensional flowline model: Journal of Glaciology, v. 44, no. 147, p. 383-393.